RESEARCH ARTICLE

Beyond mean value analysis – a voxel-based analysis of the quantitative MR biomarker water T_2 in the presence of fatty infiltration in skeletal muscle tissue of patients with neuromuscular diseases

Sarah Schlaeger[1] [ID] | Dominik Weidlich[2] [ID] | Agnes Zoffl[1] |
Edoardo Aitala Becherucci[1] | Elisabeth Kottmaier[1,2] | Federica Montagnese[3] |
Marcus Deschauer[4] | Benedikt Schoser[3] | Claus Zimmer[1] | Thomas Baum[1] |
Dimitrios C. Karampinos[2] | Jan S. Kirschke[1]

[1]Department of Diagnostic and Interventional Neuroradiology, School of Medicine, Klinikum rechts der Isar, Technical University of Munich, Munich, Germany

[2]Department of Diagnostic and Interventional Radiology, School of Medicine, Klinikum rechts der Isar, Technical University of Munich, Munich, Germany

[3]Department of Neurology, Friedrich-Baur-Institute, LMU Munich, Munich, Germany

[4]Department of Neurology, School of Medicine, Klinikum rechts der Isar, Technical University of Munich, Munich, Germany

Correspondence
Sarah Schlaeger, Department of Diagnostic and Interventional Neuroradiology, Klinikum rechts der Isar, Ismaninger Street 22, 81675, Munich, Germany.
Email: sarah.schlaeger@tum.de

The main pathologies in the muscles of patients with neuromuscular diseases (NMD) are fatty infiltration and edema. Recently, quantitative magnetic resonance (MR) imaging for determination of the MR biomarkers proton density fat fraction (PDFF) and water T_2 (T_{2w}) has been advanced. Biophysical effects or pathology can have different effects on MR biomarkers. Thus, for heterogeneously affected muscles, the routinely performed mean or median value analyses of MR biomarkers are questionable. Our work presents a voxel-based histogram analysis of PDFF and T_{2w} images to point out potential quantification errors. In 12 patients with NMD, chemical-shift encoding-based water-fat imaging for PDFF and T_2 mapping with spectral adiabatic inversion recovery (SPAIR) for T_{2w} determination was performed. Segmentation of nine thigh muscles was performed bilaterally (n = 216). PDFF and T_2 maps were coregistered. A voxel-based comparison of PDFF and T_{2w} showed a decreased T_{2w} with increasing PDFF. Mean T_{2w} and mean $T_{2w}^{\text{without fatty voxels}}$ (PDFF < 10%) show good agreement, whereas standard deviation (σ) T_{2w} and σ $T_{2w}^{\text{without fatty voxels}}$ show increasing difference with increasing values of σ. Thereby two subgroups can be observed, referring to muscles in which the exclusion of fatty voxels has a negligible influence versus muscles in which a strong dependency of the T_{2w} value distribution on the exclusion of fatty voxels is present. Because of the two opposite effects that influence T_{2w} in a voxel, namely, (i) a pathophysiologically increased water mobility leading to T_{2w} elevation, and (ii) a dependency of T_{2w} on the PDFF leading to decreased T_{2w}, the T_{2w} distribution within a muscle might be

---

- -

heterogenous and the routine mean or median analysis can lead to a misinterpretation of the muscle health. It was concluded that muscle T_{2w} mean values can wrongly suggest healthy muscle tissue. A deeper analysis of the underlying value distribution is necessary. Therefore, a quantitative analysis of T_{2w} histograms is a potential alternative.

1 | INTRODUCTION

In clinical research settings, the main pathological changes in the skeletal muscle tissue of patients with neuromuscular diseases (NMD) are atrophy or hypertrophy, fatty infiltration, and edema. Further pathologies such as skeletal muscle interstitial fibrosis are increasingly incorporated in the characterization of diseased muscle tissue. Because of its high soft tissue contrast, magnetic resonance imaging (MRI) is the modality of choice for assessment of NMD patients' muscle tissue.[1–5] Currently, in the clinical routine, qualitative sequences such as T_1- and T_2-weighted sequences with fat suppression or T_2-weighted sequences with Dixon water-fat separation are used, offering the possibility of a visual assessment of muscle pathologies.[6–8] However, assessment based on qualitative imaging is dependent on the reader's subjective judgment and expertise.[5] In particular, the assessment of subtle changes remains challenging using qualitative imaging.[9] Therefore, during the last decade, quantitative MRI techniques for determination of the MR biomarkers, proton density fat fraction (PDFF) and water T_2 (T_{2w}), have been developed.[3,10]

PDFF based on chemical-shift encoding-based water-fat MRI is considered a stable, robust, and reliable MR parameter, reflecting the tissue fat concentration, and is therefore a quantitative measure for the fatty infiltration of muscle tissue.[11] PDFF is defined as the ratio of the density of mobile protons from triglycerides (the major fat type in the body) and the total density of protons from mobile triglycerides and mobile water.[12]

T_{2w} is currently seen as a valuable MR biomarker for quantitative assessment of edema in muscle tissue, particularly as a marker for "disease activity", potentially working as a predictor for disease progression and therapy effectiveness.[10,13] T_{2w} reflects the water mobility of the muscle tissue and therefore its absolute value is more instable compared with PDFF. T_{2w} is highly sensitive to a variety of changes in the muscle microenvironment such as inflammation, necrosis, dystrophic cell lesions, denervation, tumor, and exercise of moderate to high intensity. In the context of muscle tissue in patients with NMD, a differentiation between muscle global T_2 and T_{2w} is crucial.[14] Muscle global T_2 reflects the nonchemically selective T_2 decay of muscle tissue and is therefore influenced by fat, which is of particular concern in muscles with fatty infiltration. By contrast, T_{2w} reflects the T_2 decay of muscle tissue without the influencing factor of fat. Consequently, MRI techniques for the determination of T_{2w} intend to robustly quantify T_{2w} by suppressing or separating the fat signal from the water signal. Various T_{2w} mapping techniques have been developed such as combining multi-echo spin echo (MESE) sequences with the Dixon water-fat separation technique[15] or postprocessing MESE data with multiexponential fitting models or extended phase graph (EPG) simulations.[16–19] Recently, a T_2-prepared 3D turbo spin echo (TSE) sequence with spectral adiabatic inversion recovery (SPAIR) fat suppression was presented, and it showed a good correlation of T_{2w} to the reference standard magnetic resonance spectroscopy (MRS).[20–23]

For analysis of quantitative MRI data, usually the skeletal muscles of interest are segmented, and subsequently a mean value analysis of the MR biomarkers throughout the whole muscle volume is performed.[24] In this context, the determination of the mean value is correct under the assumption of a normal distribution, whereas a median value analysis is more appropriate in the presence of a simple skewed distribution. However, it is known that biophysical effects and pathological changes that influence the muscle microenvironment can have different and complex impacts on MR biomarker distributions within a muscle. For example, it was shown that (^{1}H MRS-based) T_{2w} is decreased with increasing (^{1}H MRS-based) PDFF.[19,23,25] The dependency of T_{2w} on the fat fraction (FF) is of particular interest in muscle tissue simultaneously affected by fatty infiltration and edema, as well as with remaining healthy muscle tissue. Especially for the heterogeneously affected skeletal muscles that are typically present in various NMD, the routinely performed mean or median value analyses of MR biomarkers are questionable, and a deeper analysis for complex skewed distributions is necessary. Recently, the research community has been increasingly interested in texture analysis as an alternative method for biomarker assessment in NMD.[26,27] However, texture analysis is still complex to be performed, analyzed, and interpreted.

In the present work, a voxel-based histogram analysis of the MR biomarkers PDFF and T_{2w} based on coregistered imaging data is presented. Based on chemical-shift encoding-based water-fat imaging for PDFF determination and T_2 mapping with the T_2-prepared 3D TSE with SPAIR for T_{2w} determination in 12 patients with different NMD, the presented histogram analysis attempts to point out potential quantification errors in the mean or median analysis of quantitative imaging data in NMD.

2 | METHODS

2.1 | Subjects

Twelve patients (nine females and three males; age: 56.2 ± 15.2 years) with acquired and hereditary NMD were recruited (Table 1). The NMDs were myotonic dystrophy type 2 (DM2) (n = 5), limb girdle muscular dystrophy type R1 (LGMDR1, formerly termed LGMD2A) (n = 5), and adult-onset Pompe disease (n = 2). Diagnosis was based on muscle biopsies and/or genetic testing. The study was approved by the local institutional Committee on Human Research. All patients gave written informed consent prior to study participation.

2.2 | MR measurements

The patients' bilateral thigh regions were scanned on a 3 T system (Ingenia, Philips Healthcare, Best, The Netherlands; release 5.1.8) using the whole-body coil, the built-in 12-channel posterior coil, and a 16-channel anterior coil placed on top of the hip and thigh region. Subjects were positioned in a head-first supine position. Consecutive axial stacks to cover the midthigh region on both sides were acquired. The scan protocol included a T_2-weighted 2D Dixon TSE sequence for qualitative assessment of the muscles,[8] followed by spatially resolved chemical-shift encoding-based water-fat MRI, employing a six-echo 3D spoiled gradient echo sequence with bipolar readouts,[28] and T_2 mapping, employing a T_2-prepared 3D TSE sequence with SPAIR fat suppression.[20–22] The T_2-prepared 3D TSE with SPAIR employs a flip angle train optimized for a stable signal plateau for skeletal muscle tissue. Sequence parameters are shown in Table 2.

2.3 | Postprocessing

Water-fat separation of the T_2-weighted 2D Dixon TSE images was performed online using the vendor's mDixon algorithm.[28,29] The qualitative fat and water images were only used to gain a visual, anatomical impression of the patients' muscle tissue.

The processing of the multiecho gradient echo data was performed online using the vendor's routines for PDFF mapping. After phase error correction, water-fat separation was performed based on a complex-based signal formulation employing a multipeak fat spectrum and single T_{2^*} decay correction.[30,31] A small flip angle (3°) was used to minimize T_1 bias effects (TR = 10 ms).[29]

Postprocessing of the T_2 mapping data was performed offline using Matlab (MathWorks, Natick, MA, USA; version R2017b). An exponential fit with linear least-squares was used to fit the data described by the following equation:

$$S = S_0 * e^{-\frac{T_2 Prep}{T_2}}.$$

(1)

No fitting of the baseline was performed and magnitude data were used.

TABLE 1 Patient details for patients with myotonic dystrophy type 2 (DM2), limb girdle muscular dystrophy type R1 (LGMDR1), and adult-onset Pompe disease

Patient ID	Sex	Age (y)	BMI (kg/m^2)	Disease	Years since diagnosis
01	m	52	29.0	DM2	1
02	f	54	*	DM2	1
03	f	61	29.3	DM2	4
04	f	63	26.6	DM2	12
05	f	66	33.1	DM2	11
06	m	26	22.9	LGMDR1	2
07	f	45	24.9	LGMDR1	32
08	f	47	19.7	LGMDR1	3
09	f	49	41.3	LGMDR1	11
10	f	52	28.0	LGMDR1	5
11	f	76	21.3	Adult Pompe disease	26
12	m	84	20.8	Adult Pompe disease	8

*Body mass index (BMI) missing for this patient.

TABLE 2 Sequence parameters for the T_2-weighted 2D Dixon turbo spin echo (TSE), the six-echo 3D spoiled gradient echo, and the T_2-prepared 3D TSE sequence with spectral adiabatic inversion recovery (SPAIR)

	T_2-weighted 2D Dixon TSE	Six-echo 3D spoiled grading echo sequence	T_2-prepared 3D TSE with SPAIR
TR (ms)	3725	10	1500
TE (ms)	100	1.17	19
ΔTE (ms)	1.0	0.9	-
Number of slices	26	30	30
Slice gap (mm)	6	0	0
Acquisition voxel (mm^3)	2.5 x 2.5 x 6.0	3.2 x 2.0 x 8.0	2.0 x 2.0 x 8.0
Recon voxel (mm$^{2/3}$)	0.88 x 0.88	0.82 x 0.82 x 4.0	0.82 x 0.82 x 4.0
T2 preparation durations (ms)	-	-	20/30/40/50/60
RF-pulses (in readout)	-	Flip angle of 3°	Flip angle modulated TSE readout (echo spacing: 2.4 ms, 5 start-up echos)
TSE factor	45	-	50
Averages	2	1	Partial averaging (1.4)
FOV (mm^3)	330 x 450 x 306	260 x 420 x 120	420 x 260 x 120
Scan duration (min:s)	2:07	0:20	4:30
SENSE	-	In L/R direction, reduction factor 2	In A/P direction, reduction factor 2

Abbreviations: A/P, anterior/posterior; FOV, field of view; L/R, left/right; SENSE, sensitivity encoding.

2.4 | Image registration

3D image registration was performed using elastix (Image Sciences Institute, University Medical Center Utrecht, The Netherlands; 5.0.1),[32,33] for example, to compensate involuntary motion of the subjects between scans to allow a voxel-based comparison of PDFF and T_2 maps. The water image of the six-echo 3D spoiled gradient echo sequence represented the fixed image, whereas the first echo of the T_2-prepared 3D TSE sequence worked as a moving image. An affine transformation was applied (details are provided in the supporting information). Using the resulting transformation parameters, the postprocessed T_2 maps were registered on the PDFF maps with transformix (part of the elastix software).

2.5 | Muscle segmentation

Segmentation of the thigh muscles was performed using the Medical Imaging Interaction Toolkit (https://www.mitk.org/wiki/The_Medical_Imaging_Interaction_Toolkit_(MITK)); German Cancer Research Center, Division of Medical and Biological Informatics, Medical Imaging Interaction Toolkit, Heidelberg, Germany). Manual regions of interest (ROIs) were placed in axial slices of the PDFF maps to separately enclose nine thigh muscles: biceps femoris, gracilis, rectus femoris, sartorius, semimembranosus, semitendinosus, vastus intermedius, vastus lateralis, and vastus medialis muscles of the left and right thigh, respectively (216 muscles in total). Segmentation was performed on ten consecutive slices at the mid-thigh region, with the ROIs being placed at the outer muscle contour by a radiologist (with three years of experience). The outer muscle contour was chosen to ensure acceptable intrareader and interreader reproducibility based on the work performed by Greve et al.[34] Prior to subsequent analysis, the outermost voxels of the masks were automatically excluded to guarantee inclusion of mere muscle tissue. Bilateral muscle-specific PDFF values and T_{2w} values of the coregistered T_2 maps were extracted, enabling a voxel-based comparison of PDFF and T_{2w}.

2.6 | Data analysis

Voxel-based data analysis and plotting of the quantitative imaging data was performed using Matlab (MathWorks).

For the combined T_{2w} and PDFF analysis, a cutoff level of PDFF 60% was selected based on previous work by Schlaeger et al.[23] In this study, a PDFF of 60% was the limit where important differences in T_{2w} could be observed. Also, in the Mercuri grading scale, muscles with fatty infiltration of more than 60% are graded as severely fatty infiltrated.[2]

Voxels with fatty infiltration were defined as voxels with a PDFF of 10% or more based on the work by Inhuber et al.[35] Two different muscle mean and standard deviation (σ) T_{2w} were calculated: (i) muscle mean and σ T_{2w} incorporating all voxels of the whole muscle volume, and

(ii) muscle mean and σ T_{2w} incorporating only voxels without fatty infiltration (PDFF < 10%). Corresponding intercept and slope of the linear regression fit as well as Bland–Altman plots were calculated.

To further describe the T_{2w} distribution, a threshold of 3.4 ms was set, defining a relevant difference between σ T_{2w} and σ $T_{2w}^{\text{without fatty voxels}}$. The threshold of 3.4 ms was chosen based on measurements in ten healthy volunteers' thigh muscles with the T_2-prepared 3D TSE sequence with SPAIR.[20] Thereby, the threshold of 3.4 ms represents two times the maximal σ of T_{2w} values in the measured healthy thigh muscles. Based on the threshold of 3.4 ms and the equation,

$$\Delta_{\sigma} = \sigma\,T_{2w} - \sigma\,T_{2w}^{\text{without fatty voxels}}, \tag{2}$$

two different subgroups of T_{2w} distributions can be distinguished: (i) a subgroup where $\Delta_{\sigma} \leq 3.4$ ms is indicating that the exclusion of fatty voxels (PDFF $\geq$ 10%) has a negligible influence on the T_{2w} value distribution; and (ii) a subgroup where if $\Delta_{\sigma} > 3.4$ ms is indicating a strong dependency of the T_{2w} value distribution on the exclusion of fatty voxels. The two subgroups were compared with regard to the skewness of the T_{2w} histogram using a boxplot analysis and a Mann–Whitney U-test.

3 | RESULTS

Figure 1 shows representative PDFF and T_2 maps in a patient with DM2, LGMDR1, and adult-onset Pompe disease, respectively. Disease-characteristic patterns of muscle fatty infiltration are visible. In particular, the hamstring muscles of the Pompe patient are heterogeneously affected by fatty infiltration and edema, which is reflected by varying PDFF and T_{2w} values.

The voxel-based comparison of coregistered PDFF and T_{2w} values revealed a dependency of T_{2w} on the FF, showing that T_{2w} is decreased with increasing PDFF (Figure 2A). Figure 2B shows that decreased T_{2w} with increasing PDFF can be observed independently in all the investigated patient groups (DM2, LGMDR1, and Pompe disease).

A more detailed comparison of the T_{2w} value distribution in the semimembranosus muscle of (i) a patient with Pompe disease and (ii) a patient with DM2 revealed different histograms, as shown in Figure 3. Both semimembranosus muscles approximately have the same mean T_{2w} (≈ 31 ms). However, the Pompe patient's T_{2w} histogram has a broad distribution, and two main peaks are present (at 22 and 35 ms) corresponding to T_{2w} of edematous and fatty voxels, whereas in the DM2 patient's T_{2w} histogram, a single peak is present (at 31 ms) corresponding to T_{2w} of healthy voxels.

A combined assessment of T_{2w} and PDFF in the histogram of the semimembranosus muscle of the Pompe patient reveals that the two main peaks (at 22 and 35 ms) generally correspond to different underlying PDFF regimes (PDFF > 60% and $\leq$60%), whereas the single peak in the
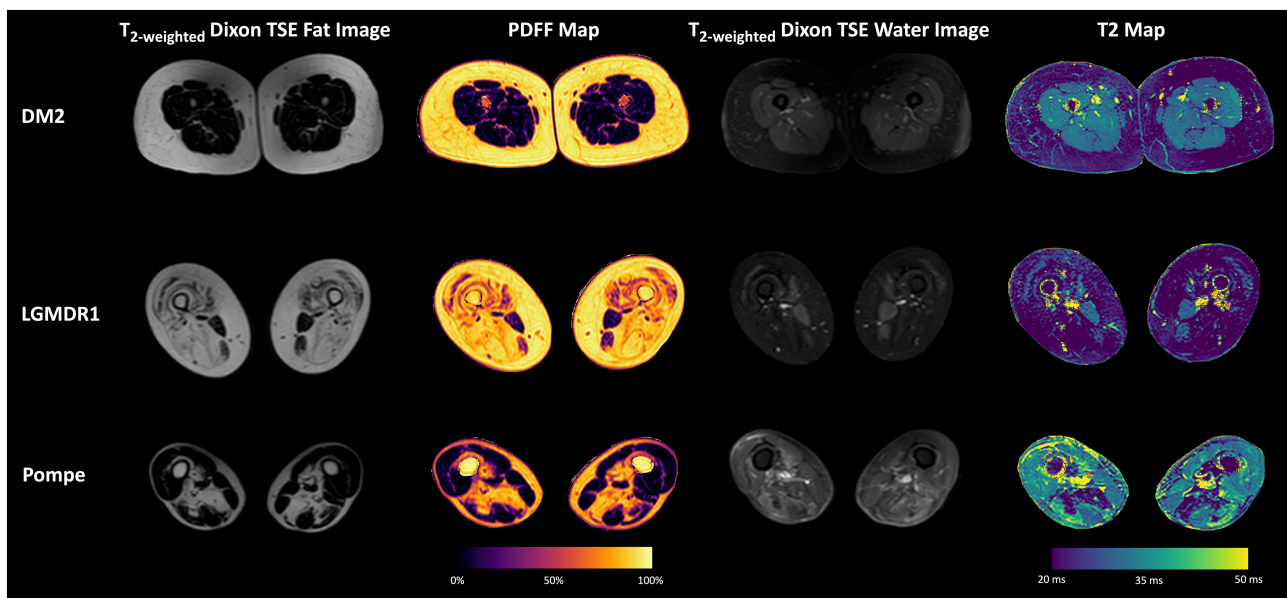

FIGURE 1 Representative water T_2 ($T_{2\text{-weighted}}$) Dixon turbo spin echo (TSE) fat and water images, proton density fat fraction (PDFF) maps and T_2 maps of a patient with mytonic dystrophy type 2 (DM2), limb girdle muscular dystrophy type R1 (LGMDR1), and adult-onset Pompe disease
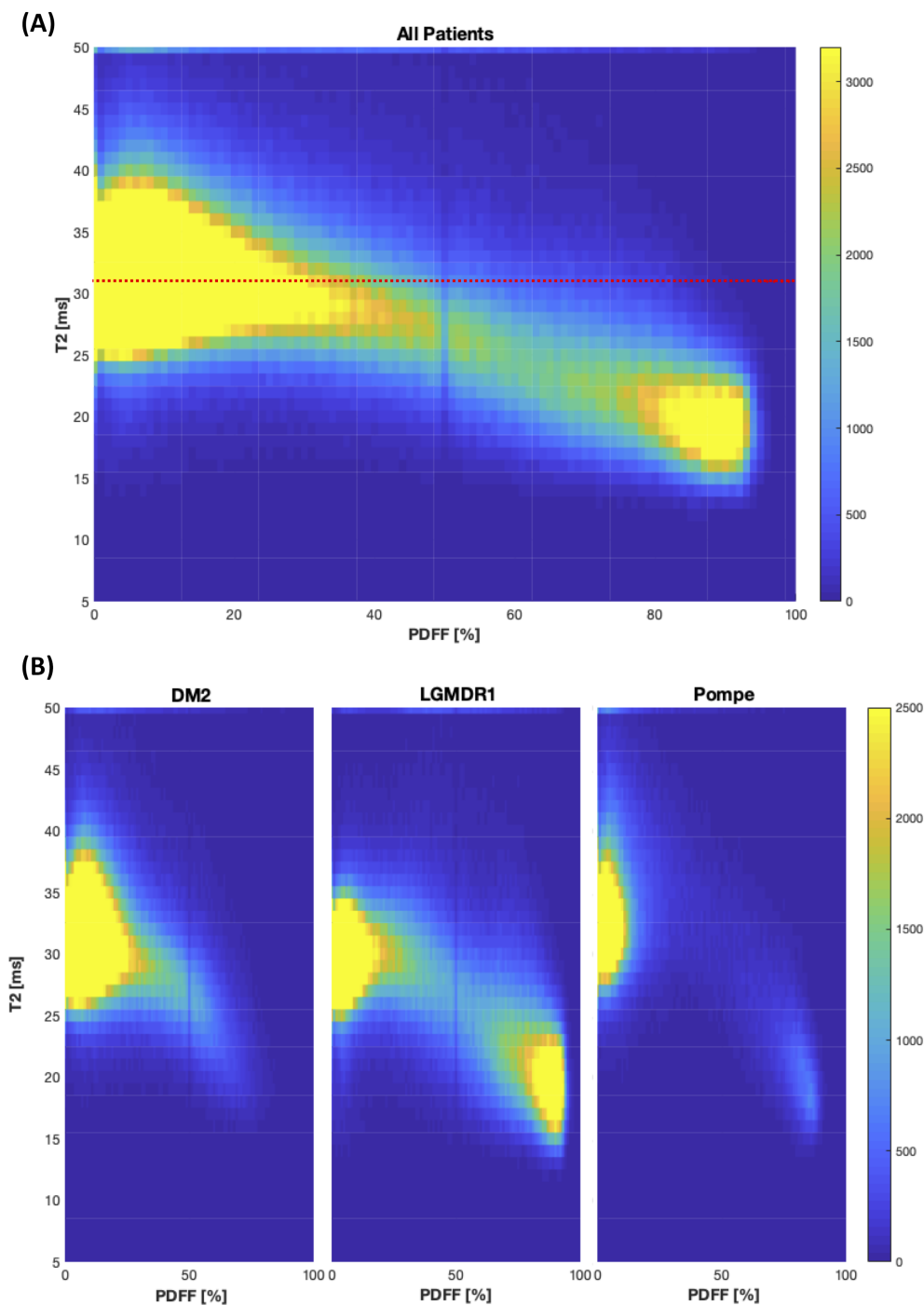
(A)

(B)

FIGURE 2 Histogram of certain proton density fat fraction (PDFF)/water T_2 (T_{2w}) value combinations (the brightness encodes the probability). (A) Decreased T_{2w} with increasing PDFF in 216 muscles of patients with neuromuscular diseases. For comparison, the mean T_{2w} of healthy thigh muscle tissue measured with the T_2 mapping sequence employed in the work performed by Klupp et al. is indicated as a red line ($\approx$ 31 ms).[20] (B) Behavior of T_{2w} with increasing PDFF separated for three different patient groups (mytonic dystrophy type 2 [DM2], limb girdle muscular dystrophy type R1 [LGMDR1], and adult-onset Pompe disease)

histogram of the semimembranosus muscle of the DM2 patient at 31 ms corresponds to only one PDFF regime (PDFF $\leq$ 60%). For comparison, the respective histogram of the semimembranosus muscle of a LGMD1R patient also shows a single peak, however at 21 ms corresponding to the PDFF > 60 % regime (Figure 4).

Figure 5 shows the results of a pooled analysis of the data from all 216 muscles. A linear regression between mean T_{2w} and mean $T_{2w}^{without\ fatty\ voxels}$ shows a slope of 0.7 and an intercept of 10.64 ms (Figure 5A). In the corresponding Bland–Altmann plot (Figure 5B), almost all the datapoints are within the 95% confidence interval (CI). When comparing σT_{2w} and $\sigma T_{2w}^{without\ fatty\ voxels}$, the linear regression shows a slope of
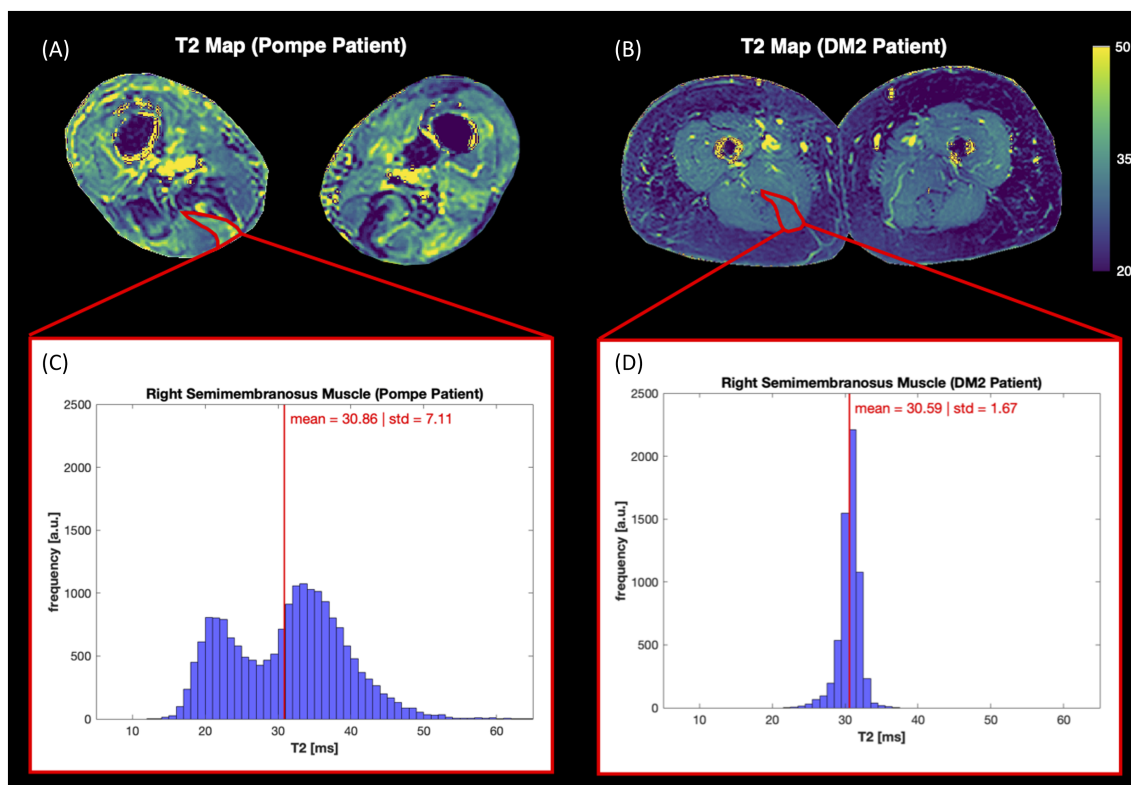
FIGURE 3 T_2 maps of the thigh muscles of (A) a patient with adult-onset Pompe disease and (B) a patient with mytonic dystrophy type 2 (DM2). Segmentation masks of the right semimembranosus muscle are depicted in red, respectively. Corresponding histograms of water T_2 (T_{2w}) in the right semimembranosus muscle of (C) the patient with adult-onset Pompe disease and (D) the patient with DM2. In the left histogram (C) two peaks are present (at 22 and 35 ms) (number of bins: 55), whereas in the right histogram (D) only one peak is present (at 31 ms) (number of bins: 30); however, both muscles have approximately the same mean T_{2w} ($\approx$ 31 ms)
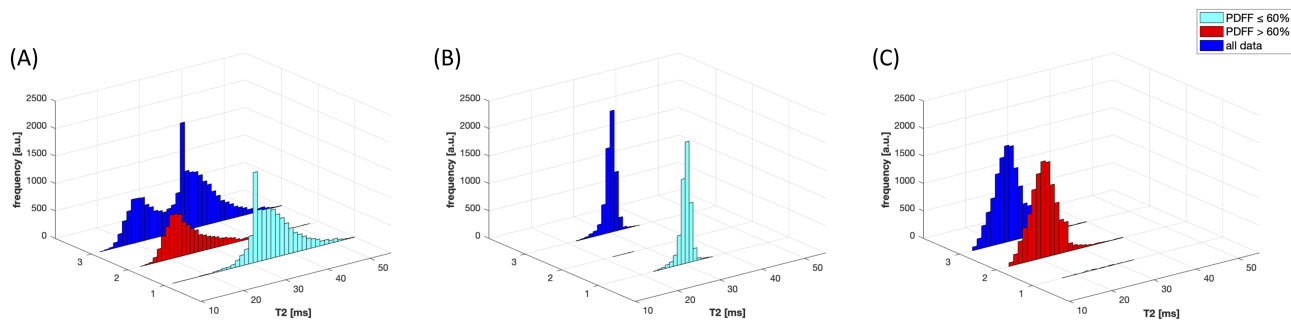

FIGURE 4 Combined assessment of water T_2 (T_{2w}) and proton density fat fraction (PDFF) in the histogram of the semimembranosus muscle of (A) the Pompe patient and (B) the mytonic dystrophy type 2 (DM2) patient. For comparison, additionally, in (C) the histogram of the semimembranosus muscle of a limb girdle muscular dystrophy type R1 (LGMDR1) patient is shown. In (A), the two peaks (at 22 and 35 ms) mainly correspond to different underlying PDFF regimes (PDFF > 60% and ≤60%) (number of bins: 55 [PDFF ≤ 60%]; 41 [PDFF > 60%]; 55 [all data]). In (B), the single peak at 31 ms corresponds to only one PDFF regime (PDFF ≤ 60%) (number of bins: 15/15/15). In (C), the single peak at 21 ms corresponds to the second PDFF regime (PDFF > 60%) (number of bins: 25/25/25)

0.28 and an intercept of 2.37 ms (Figure 5C). In the corresponding Bland–Altman plot (Figure 5D), the difference between the two variables increases with increasing mean σ.

Based on the threshold of 3.4 ms and Equation (2) (see subsection 2.6), two different subgroups of datapoints can be distinguished. The datapoints of one subgroup (blue; Δ_σ ≤ 3.4 ms) stay within the 95% CI, indicating that in the underlying muscles the exclusion of fatty voxels has a negligible influence on the T_{2w} value distribution. As many datapoints of the second subgroup (red; Δ_σ > 3.4 ms) exceed the 95% CI, a strong dependency of the T_{2w} value distribution on the exclusion of fatty voxels in the corresponding muscles can be observed.
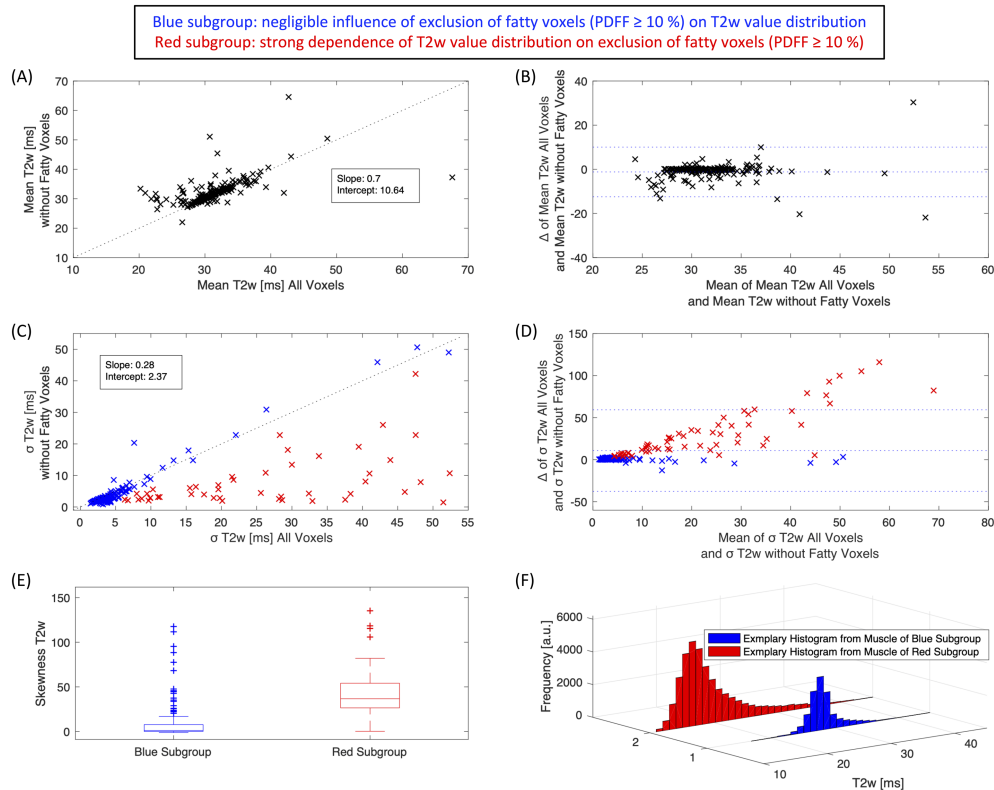
FIGURE 5 Pooled analysis of the data from all 216 muscles. In general, two different subgroups of datapoints can be distinguished: (i) a subgroup where, in the underlying muscles, the exclusion of fatty voxels has a negligible influence on the water T_2 (T_{2w}) value distribution (blue), and (ii) a subgroup where a strong dependency of the T_{2w} value distribution on the exclusion of fatty voxels in the corresponding muscles can be observed (red). (A) A linear regression between mean T_{2w} and mean $T_{2w}^{\text{without fatty voxels}}$ shows a slope of 0.7 and an intercept of 10.64 ms. (B) In the corresponding Bland–Altmann plot, almost all the datapoints are within the 95% confidence interval (CI). (C) A linear regression between σ T_{2w} and σ $T_{2w}^{\text{without fatty voxels}}$ shows a slope of 0.28 and an intercept of 2.37 ms. (D) In the corresponding Bland–Altman plot, the difference between the two variables increases with increasing mean σ. (E) Based on the equation $\Delta_\sigma = \sigma\, T_{2w} - \sigma\, T_{2w}^{\text{without fatty voxels}}$, two different subgroups can be distinguished, which correspond to two different skewness distributions (blue: $\Delta_\sigma \leq 3.4$ ms; red: $\Delta_\sigma > 3.4$ ms). (F) An exemplary T_{2w} histogram of the left rectus femoris muscle of a patient with limb girdle muscular dystrophy type R1 (LGMDR1) corresponds to the blue subgroup, and an exemplary T_{2w} histogram of the left biceps femoris muscle of another patient with LGMDR1 corresponds to the red subgroup (number of bins: 35)

To further investigate the blue and red subgroups, the skewness of the T_{2w} histograms for muscles of both subgroups was calculated. Figure 5E shows the corresponding boxplot analysis. The difference in skewness T_{2w} between the muscles of the two subgroups is highly significant ($p < 0.01$): the muscles of the blue subgroup have a rather small skewness (median: 1.11), whereas the muscles of the red subgroup have a high and positive skewness (median: 36.70). Figure 5F shows exemplary T_{2w} histograms for a muscle of the blue and red subgroup, respectively. The T_{2w} histogram of the muscle of the blue subgroup has a single peak, corresponding to a small skewness, whereas the T_{2w} histogram of the muscle from the red subgroup has a broad distribution with the peak shifted to the left and a tail on the right, corresponding to a positive skewness.

Mean, standard deviation, median and range of PDFF, T_{2w} and $T_{2w}^{\text{without fatty voxels}}$ for each muscle in every patient are shown in Table S1. Additionally, skewness of T_{2w} values within each muscle, as well as the number of voxels in the segmentation mask including and excluding fatty voxels, are shown.

4 | DISCUSSION

Based on coregistered PDFF and T_{2w} imaging data from 12 patients with different NMD, the present work shows the impact of two opposite effects on the T_{2w} value in a single voxel: (i) a pathophysiologically increased water mobility leading to T_{2w} elevation and (ii) a dependency of T_{2w} on the FF leading to decreased T_{2w} with increasing FF. The present work demonstrates the quantification errors that result from a simple mean or median analysis of the MR biomarkers by presenting a voxel-based histogram analysis of T_{2w} and PDFF.

The recent progress in the development of quantitative imaging techniques for MR biomarker determination in patients with NMD requires further consideration regarding the appropriate assessment of PDFF and T_{2w} as MR biomarkers. As the present routinely performed analysis of quantitative MR biomarkers in NMD is based on a mean or median value calculation of PDFF and T_{2w} for a muscle of interest, the influence of partial volume effects and regional pathological differences on the MR biomarkers analysis is neglected. However, the present work reveals a potential misinterpretation of muscle health when only the mean T_{2w} value of a heterogeneously affected muscle is assessed. In a heterogeneously affected muscle with healthy, edematous, and fatty voxels, the two opposite effects leading to elevated and reduced T_{2w} values might lead to a muscle mean T_{2w} similar to the mean T_{2w} of a healthy muscle, as high and low T_{2w} values are canceling each other out. Because T_{2w} elevation reflecting increased water mobility in a variety of circumstances such as inflammation, denervation, or exercise is the alteration desired to be measured during T_{2w} mapping, the present work focused on the effect of fat on the T_{2w} distribution in a muscle volume.

Previous work showed a dependency of T_{2w} and PDFF, increasing the attention given to biophysical and pathological microenvironmental effects that influence absolute T_{2w} values.[19,23,25] The present work confirms the observation that T_{2w} is decreased with increasing FF based on imaging sequences. Exchange and compartmentalization of the T_2 decay or susceptibility differences between muscle water and fat might contribute to the observed T_{2w} behavior.[23]

Because of decreased T_{2w} values with increasing PDFF, a T_{2w} histogram of a muscle with remaining healthy muscle tissue that is simultaneously affected by fatty infiltration shows at least two peaks of the underlying T_{2w} distribution corresponding to different PDFF regimes. In general, two different types of muscles can be distinguished: (i) muscles in which the exclusion of fatty voxels has a negligible influence on the σ T_{2w}, and (ii) muscles in which a strong dependency of the T_{2w} value distribution on the exclusion of fatty voxels can be observed. Consequently, muscles of the first type (i) show no or a homogeneous fatty infiltration, whereas muscles of the second type (ii) show heterogeneous fatty infiltration throughout the muscle volume, leading to a nonnormal distribution of T_{2w} values, which is also represented in a low (first type) or a high, positive (second type) skewness of the T_{2w} histogram.

Subsequently, the assessment of muscle pathologies based on the MR biomarkers T_{2w} and PDFF might require an interpretation beyond mean or median value analysis. An analysis of the form of the underlying T_{2w} value distribution as well as correlations and effects between the MR biomarkers is necessary, such as an analysis of skewness or bimodality. The present work is meant to demonstrate the disadvantages of mere mean value determination. The implementation of quantitative histogram analysis is one way to overcome the disadvantages of a mean or median value determination by providing insights into the exact frequency distribution of different T_{2w} values within an ROI.

Additionally, the current work emphasizes the necessity for a more precise definition of pathological, specifically elevated T_{2w} values, to foster a feasible approach for implementation of MR biomarkers in the clinical routine of NMD patients. Because the FF has an influence on the absolute T_{2w} value, two important aspects have to be taken into consideration: (i) a threshold definition for pathological (elevated) T_{2w} has to be forwarded, particularly for fatty infiltrated muscles. Based on the work by Klupp et al.,[20] measurements in the thigh muscles of healthy volunteers revealed a physiological T_{2w} of max. 31.4 ± 1.7 ms (rectus femoris) using the T_2-prepared 3D TSE sequence with SPAIR.[20] Based on this work, a T_{2w} above the threshold plus standard deviation might be considered to be elevated. However, because of decreased T_{2w} values with increasing PDFF, a T_{2w} below the proposed threshold might also reflect elevated T_{2w} values, because of the two counteracting effects of T_{2w} elevation due to increased water mobility and T_{2w} decrease due to fatty infiltration; and (ii) in highly fatty infiltrated muscles, in particular in voxels with PDFF values of more than 60%, T_{2w} seems to be substantially decreased, which might render its significance for increased water mobility assessment impossible. Consequently, in future T_{2w} biomarkers analysis, voxels with PDFF values of more than 60% might need to be analyzed separately from the main analysis, reducing the volume of interest for T_{2w} analysis to voxels with a PDFF of 60% or less. Both aspects currently lack comparison with reference standard measurements for their clinical relevance, thus longitudinal evaluations of the MR biomarkers T_{2w} and PDFF, their interaction and their significance for disease progression and response to treatment are needed.

The current study has some limitations. First, a small number of patients was included in the study. This was mainly because of the rare character of NMD. Because the present work focuses on a voxel-based assessment of PDFF and T_{2w}, datapoints were available from 216 muscles in total, although values from the same patient could not be treated as though they were independent. In particular, only two Pompe patients could be included in the present study; however, they display highly interesting T_{2w} distributions due to their very heterogeneously affected muscle tissue.[36,37] To summarize, the present work is mainly meant to be methodological and descriptive and does not intend to offer conclusions about characteristic MR biomarker distributions within different NMD. Second, the proposed histogram analysis does not offer information about spatial distribution of the different MR biomarkers values within the muscle volume. Spatial information is of particular interest, as recently, regional variations between PDFF in proximal, central, and distal parts of the thigh muscles have been shown.[34] Third, as mentioned before, because of the lack of a real reference standard measurement technique, longitudinal analysis of the MR biomarkers is necessary. Fourth, the presented results are specific to the employed MR sequences and to the investigated T_2 regime due to the low resolution in the TE dimension. Therefore, also the threshold of 3.4 ms, which represents two times the maximal σ of T_{2w} values in healthy thigh muscles using the employed MR sequence, is highly specific and based on a small number of previous measurements. However, the threshold is meant as an approach to define a relevant difference between σ T_{2w} and σ $T_{2w}^{\text{without fatty voxels}}$. A generalization of the findings to different T_{2w} and PDFF mapping sequences is likely. Fifth, the spatial

resolution of the employed quantitative MR sequences is relatively low, which generally facilitates partial volume effects. However, the sequence parameters were chosen to allow fast protocols, also appropriate for a clinical implementation. Thus the shown quantification errors also have to be taken into consideration when the employed T_2 mapping sequence is applied in the clinical routine.

5 | CONCLUSION

The present work demonstrates the two opposite effects on T_{2w} in a single voxel based on coregistered quantitative MRI data: (i) a pathophysiologically increased water mobility leading to T_{2w} elevation and (ii) a dependency of T_{2w} on the FF leading to decreased T_{2w} with increasing FF. Therefore, the assessment of muscle pathologies based on PDFF and T_{2w} requires an interpretation beyond mean or median value analysis to account for regional pathological differences and the resulting quantification errors. A deeper analysis of the underlying value distributions is necessary. Therefore, a quantitative analysis of T_{2w} histograms is a potential alternative.

CONFLICT OF INTEREST
JSK is co-founder of Bonescreen GmbH.

ORCID
Sarah Schlaeger (iD) https://orcid.org/0000-0002-2736-9225
Dominik Weidlich (iD) https://orcid.org/0000-0001-7842-2682

REFERENCES
1. Mercuri E, Jungbluth H, Muntoni F. Muscle imaging in clinical practice: diagnostic value of muscle magnetic resonance imaging in inherited neuromuscular disorders. *Curr Opin Neurol*. 2005;18(5):526-537. doi:10.1097/01.wco.0000183947.01362.fe
2. Mercuri E, Pichiecchio A, Allsop J, Messina S, Pane M, Muntoni F. Muscle MRI in inherited neuromuscular disorders: past, present, and future. *J Magn Reson Imaging*. 2007;25(2):433-440. doi:10.1002/jmri.20804
3. Wattjes MP, Kley RA, Fischer D. Neuromuscular imaging in inherited muscle diseases. *Eur Radiol*. 2010;20(10):2447-2460. doi:10.1007/s00330-010-1799-2
4. Hollingsworth KG, de Sousa PL, Straub V, Carlier PG. Towards harmonization of protocols for MRI outcome measures in skeletal muscle studies: consensus recommendations from two TREAT-NMD NMR workshops, 2 May 2010, Stockholm, Sweden, 1-2 October 2009, Paris, France. *Neuromuscul Disord*. 2012;22(Suppl 2):S54-S67. doi:10.1016/j.nmd.2012.06.005
5. Leung DG. Magnetic resonance imaging patterns of muscle involvement in genetic muscle diseases: a systematic review. *J Neurol*. 2017;264(7): 1320-1333. doi:10.1007/s00415-016-8350-6
6. Straub V, Carlier PG, Mercuri E. TREAT-NMD workshop: pattern recognition in genetic muscle diseases using muscle MRI: 25-26 February 2011, Rome, Italy. *Neuromuscul Disor*. 2012;22(Suppl 2):S42-S53. doi:10.1016/j.nmd.2012.08.002
7. Ten Dam L, van der Kooi AJ, Verhamme C, Wattjes MP, de Visser M. Muscle imaging in inherited and acquired muscle diseases. *Eur J Neurol*. 2016; 23(4):688-703. doi:10.1111/ene.12984
8. Schlaeger S, Klupp E, Weidlich D, et al. T2-weighted Dixon turbo spin echo for accelerated simultaneous grading of whole-body skeletal muscle fat infiltration and edema in patients with neuromuscular diseases. *J Comput Assist Tomogr*. 2018;42(4):574-579. doi:10.1097/rct.0000000000000723
9. Schlaeger S, Sollmann N, Zoffl A, et al. Quantitative muscle MRI in patients with neuromuscular diseases—association of muscle proton density fat fraction with semi-quantitative grading of fatty infiltration and muscle strength at the thigh region. *Diagnostics*. 2021;11(6):1056. doi:10.3390/diagnostics11061056
10. Carlier PG, Marty B, Scheidegger O, et al. Skeletal muscle quantitative nuclear magnetic resonance imaging and spectroscopy as an outcome measure for clinical trials. *J Neuromuscul Dis*. 2016;3(1):1-28. doi:10.3233/jnd-160145
11. Reeder SB, Hu HH, Sirlin CB. Proton density fat-fraction: a standardized MR-based biomarker of tissue fat concentration. *J Magn Reson Imaging*. 2012; 36(5):1011-1014. doi:10.1002/jmri.23741
12. Hu HH, Li Y, Nagy TR, Goran MI, Nayak KS. Quantification of absolute fat mass by magnetic resonance imaging: a validation study against chemical analysis. *Int J Body Compos Res*. 2011;9(3):111-122.
13. Kim HK, Laor T, Horn PS, Racadio JM, Wong B, Dardzinski BJ. T2 mapping in Duchenne muscular dystrophy: distribution of disease activity and correlation with clinical assessments. *Radiology*. 2010;255(3):899-908. doi:10.1148/radiol.10091547
14. Carlier PG. Global T2 versus water T2 in NMR imaging of fatty infiltrated muscles: different methodology, different information and different implications. *Neuromuscul Disord*. 2014;24(5):390-392. doi:10.1016/j.nmd.2014.02.009
15. Janiczek RL, Gambarota G, Sinclair CD, et al. Simultaneous T_2 and lipid quantitation using IDEAL-CPMG. *Magn Reson Med*. 2011;66(5):1293-1302. doi:10.1002/mrm.22916
16. Marty B, Baudin P-Y, Reyngoudt H, et al. Simultaneous muscle water T2 and fat fraction mapping using transverse relaxometry with stimulated echo compensation. *NMR Biomed*. 2016;29(4):431-443. doi:10.1002/nbm.3459

17. Lebel RM, Wilman AH. Transverse relaxometry with stimulated echo compensation. *Magn Reson Med*. 2010;64(4):1005-1014. doi:10.1002/mrm.22487

18. Azzabou N, Loureiro de Sousa P, Caldas E, Carlier PG. Validation of a generic approach to muscle water T2 determination at 3T in fat-infiltrated skeletal muscle. *J Magn Reson Imaging*. 2015;41(3):645-653. doi:10.1002/jmri.24613

19. Santini F, Deligianni X, Paoletti M, et al. Fast open-source toolkit for water T2 mapping in the presence of fat from multi-echo spin-echo acquisitions for muscle MRI. *Front Neurol*. 2021;12(248). doi:10.3389/fneur.2021.630387

20. Klupp E, Weidlich D, Schlaeger S, et al. B1-insensitive T2 mapping of healthy thigh muscles using a T2-prepared 3D TSE sequence. *PLoS One*. 2017;12(2):e0171337 doi:10.1371/journal.pone.0171337

21. Weidlich D, Schlaeger S, Kooijman H, et al. T2 mapping with magnetization-prepared 3D TSE based on a modified BIR-4 T2 preparation. *NMR Biomed*. 2017;30(11):e3773. doi:10.1002/nbm.3773

22. Schlaeger S, Weidlich D, Klupp E, et al. Water T2 mapping in fatty infiltrated thigh muscles of patients with neuromuscular diseases using a T2-prepared 3D turbo spin echo with SPAIR. *J Magn Reson Imaging*. 2020;51(6):1727-1736. doi:10.1002/jmri.27032

23. Schlaeger S, Weidlich D, Klupp E, et al. Decreased water T(2) in fatty infiltrated skeletal muscles of patients with neuromuscular diseases. *NMR Biomed*. 2019;32(8):e4111. doi:10.1002/nbm.4111

24. Willcocks RJ, Arpan IA, Forbes SC, et al. Longitudinal measurements of MRI-T2 in boys with Duchenne muscular dystrophy: effects of age and disease progression. *Neuromuscul Disord*. 2014;24(5):393-401. doi:10.1016/j.nmd.2013.12.012

25. Keene KR, Beenakker JM, Hooijmans MT, et al. T(2) relaxation-time mapping in healthy and diseased skeletal muscle using extended phase graph algorithms. *Magn Reson Med*. 2020;84(5):2656-2670. doi:10.1002/mrm.28290

26. Akinci D'Antonoli T, Santini F, Deligianni X, et al. Combination of quantitative MRI fat fraction and texture analysis to evaluate spastic muscles of children with cerebral palsy. *Front Neurol*. 2021;12:633808. doi:10.3389/fneur.2021.633808

27. Diaz-Manera J, Pichiecchio A, Santini F, Filosto M. Editorial: Imaging of neuromuscular diseases. *Front Neurol*. 2021;12. doi:10.3389/fneur.2021.814579

28. Liu CY, McKenzie CA, Yu H, Brittain JH, Reeder SB. Fat quantification with IDEAL gradient echo imaging: correction of bias from T(1) and noise. *Magn Reson Med*. 2007;58(2):354-364. doi:10.1002/mrm.21301

29. Karampinos DC, Yu H, Shimakawa A, Link TM, Majumdar S. T_1-corrected fat quantification using chemical shift-based water/fat separation: application to skeletal muscle. *Magn Reson Med*. 2011;66(5):1312-1326. doi:10.1002/mrm.22925

30. Yu H, Shimakawa A, McKenzie CA, Brodsky E, Brittain JH, Reeder SB. Multiecho water-fat separation and simultaneous R2* estimation with multifrequency fat spectrum modeling. *Magn Reson Med*. 2008;60(5):1122-1134. doi:10.1002/mrm.21737

31. Yu H, McKenzie CA, Shimakawa A, et al. Multiecho reconstruction for simultaneous water-fat decomposition and T2* estimation. *J Magn Reson Imaging*. 2007;26(4):1153-1161. doi:10.1002/jmri.21090

32. Klein S, Staring M, Murphy K, Viergever MA, Pluim JPW. elastix: a toolbox for intensity-based medical image registration. *IEEE Trans Med Imaging*. 2010;29(1):196-205. doi:10.1109/TMI.2009.2035616

33. Shamonin D, Bron E, Lelieveldt B, Smits M, Klein S, Staring M. Fast parallel image registration on CPU and GPU for diagnostic classification of Alzheimer's disease. *Front Neuroinform*. 2014;7(50). doi:10.3389/fninf.2013.00050

34. Greve T, Burian E, Zoffl A, et al. Regional variation of thigh muscle fat infiltration in patients with neuromuscular diseases compared to healthy controls. *Quant Imaging Med Surg*. 2021;11(6):2610-2621. doi:10.21037/qims-20-1098

35. Inhuber S, Sollmann N, Schlaeger S, et al. Associations of thigh muscle fat infiltration with isometric strength measurements based on chemical shift encoding-based water-fat magnetic resonance imaging. *Eur Radiol Exp*. 2019;3(1):45. doi:10.1186/s41747-019-0123-4

36. Carlier RY, Laforet P, Wary C, et al. Whole-body muscle MRI in 20 patients suffering from late onset Pompe disease: Involvement patterns. *Neuromuscul Disord*. 2011;21(11):791-799. doi:10.1016/j.nmd.2011.06.748

37. Carlier PG, Azzabou N, de Sousa PL, et al. Skeletal muscle quantitative nuclear magnetic resonance imaging follow-up of adult Pompe patients. *J Inherit Metab Dis*. 2015;38(3):565-572. doi:10.1007/s10545-015-9825-9

SUPPORTING INFORMATION

Additional supporting information can be found online in the Supporting Information section at the end of this article.